Indian Journal of Pure & Applied Physics
Vol. 55, August 2017, pp. 551-563

Soret and Dufour effects on MHD flow with heat and mass transfer past a permeable stretching sheet in presence of thermal radiation

G Sreedevi[a]*, D R V Prasada Rao[b], O D Makinde[c] & G Venkata Ramana Reddy[a]

[a]Department of Mathematics, K L University, Green Fields, Vaddeswaram, Guntur 522 502, India

[b]Department of Mathematics, S K University, Anantapur 515 003, India

[c]Faculty of Military Science, Stellenbosch University, Private Bag X2, Saldanha 7395, South Africa

Received 14 June 2016; accepted 3 January 2017

An analysis has been carried out to study the combined effects of the magnetic field, Joule heating, thermal radiation absorption, viscous dissipation, Buoyancy forces, thermal-diffusion and diffusion-thermion the convective heat and mass transfer flow of an electrically conducting fluid over a permeable vertically stretching sheet. The boundary layer equations for the fluid flow, heat and mass flux under consideration have been obtained and reduced into a system of non-linear ordinary differential equations by using appropriate similarity transformation. Using shooting method coupled with the fourth order Runge-Kutta integration scheme, the numerically solutions have been obtained and presented graphically. The effects of various embedded thermo-physical parameters on the fluid velocity, temperature, skin friction, Nusselt number and Sherwood number have been determined and discussed quantitatively. A comparison of a special case of our results with the one previously reported in the literature shows a very good agreement. An increase in values of thermal radiation, viscous dissipation, suction/injection coefficient and chemical reaction results in the increase of velocity, temperature and heat-mass transfer rates. It is further noted that the velocity, temperature and heat-mass transfer rates reduces on the boundary layer of a permeable vertical stretching sheet due to increase in the values of Soret or decrease in values of Dufour. Further, this work leads to study different flows of electrically conducting fluid over a permeable vertical stretching sheet problem that includes the two dimensional non-linear boundary equations.

Keywords: Joule heating, MHD, Thermal radiation, Buoyancy forces, Soret effect, Dufour effect

1 Introduction

Natural convection permeates, either be it a study of natural phenomenon like the structure of stars and planets or be it in an engineering application study say cooling of nuclear reactors. On the other hand, an increase in the temperature of a conductor by the result of resistance to the electrical current flowing through it is referred to as Joule heating. However, at an atomic level, Joule heating is the resultant of moving electrons colliding with atoms in a conductor, whereupon momentum is transferred to the atom, increasing its kinetic energy. Electro migration is when similar collisions results in a permanent structural change, rather than just an elastic response. The rise in the temperature of the conductor is due to the increase in the kinetic energy of the ions which manifests itself as heat. Accordingly, the energy is transferred from electrical power supply to the conductor and any other material that comes in thermal contact.

*Corresponding author (E-mail: sreedevihari2007@gmail.com)

The study of magneto-hydrodynamic (MHD) radiative viscous flows has gained much importance in geothermal and industrial applications such as high-temperature plasmas, cooling of nuclear reactors, liquid metal fluids, MHD accelerators and power generation systems. Advanced studies went into MHD free convective flow analyzing the effect of viscous dissipation and Joule heating with variable plate temperature[1-3]. Makinde and Chinyoka[4] examined the MHD transient flow and heat transfer in a channel with radiative heat and convective cooling. Das *et al.*[5] analyzed the effects of Joule heating and viscous dissipation on MHD mixed convective slip flow over an inclined porous plate. Makinde *et al.*[6] analyzed nanofluid in a porous medium of a convectively heated plate and studied the combined effects of variable viscosity, thermophoresis and thermal radiation on MHD boundary layer flow. The study of heat and mass transfer flow over a moving vertical plate with convective surface boundary conditions on MHD was studied by Makinde[7]. Hossain and Alim[8] examined the problem of natural convection-radiation

interaction on boundary layer flow along a vertical thin cylinder. The study of natural convection boundary layer flow of a viscous incompressible fluid along an isothermal horizontal plate with the effects of conduction-radiation interaction was done by Hossain and Takhar[9]. The study of heat transfer over a stretching surface of variable temperature under a steady nonlinear hydromagnetic flow was done by Devi and Thiyagarajan[10]. An analysis was carried out by Mukhopadhyay and Andersson[11] on the effects of slip and heat transfer analysis of flow over a stretching surface with unsteady condition. Makinde[12] further analyzed the unsteady MHD natural convection from a heated vertical plate with constant heat flux, chemical reaction and thermal radiation effects. The combined effect of thermal radiation and viscous dissipation on fluid flows on a non-linearly stretched permeable wall was studied by Cortell[13]. Makinde *et al.*[14] investigated the problem of MHD flow of a variable viscosity nanofluid over a radially stretching convective surface. The study over non-aligned MHD stagnation point flow of variable viscosity nanofluids past a stretching sheet with radiative heat was studied by Khan *et al.*[15]. The effects of thermal radiation and non-uniform heat source/sink on mixed convection flow and heat transfer over an unsteady stretching permeable sheet was advanced by Pal[16]. Sivaraj and Kumar[17] analyzed the viscoelastic fluid flow over a moving vertical cone and flat plate with variable electric conductivity. A study of different mathematical analytical methods applied on MHD permeable heat flow past stretching/shrinking two-three dimensional objects was done by Turkyilmazoglu[18].

The study of heat and mass transfer of viscous fluid over a steady stretching sheet with viscous dissipation and internal heat generation was conducted by Vajravelu and Hadjinicolaou[19]. The combined heat and mass transfer of an electrically conducting fluid in MHD natural convection, in a vertical surface with ohmic heating was studied by Chen[20]. The effects of ohmic heating and viscous dissipation on steady MHD flow near to stagnation point on an isothermal stretching sheet was studied by Sharma and Singh[21]. The combined effect of Hall current, Joule heating and thermal diffusion in a steady free convection heat and mass transfer was investigated by Singh and Gorla[22]. The combined effect of mixed convection with thermal radiation and chemical reaction on MHD flow of viscous and electrically conducting fluid past a vertical permeable surface embedded in a porous medium was analyzed by Pal and Talukdar[23]. The effects of ohmic heating and viscous dissipation was studied on mass transfer by Babu and Reddy[24] on MHD mixed convective flow over a vertical surface. Babaelahi *et al.*[25] analysed the effects of viscous and ohmic dissipation in a visco-elastic MHD fluid of a boundary layer flow over a stretching surface. Raju *et al.*[26] studied the viscous dissipation and Joule heating in a horizontal channel with insulated and impermeable bottom wall. Employing the Chebyshev finite difference method, Khader and Ahmed[27] studied the effect of viscous dissipation over a permeable stretching surface embedded in a porous medium with a second order slip. An investigation was carried out by Motsumi and Makinde[28] on the effects of thermal radiation and viscous dissipation over a permeable moving flat plate on boundary layer flow of nanofluids. Advancing studies on stretching sheet, Pal and Mondal[29] studied the viscous-ohmic dissipation on MHD convective–radiative boundary layer flow of nanofluids. The study on MHD fluid flow and heat transfer past two-dimensional porous stretching/ shrinking bodies was done by Turkyilmazoglu[30].

Soret and Dufour effects (S & D effects) are assumed to be negligible in the above studies. The mass flux created by a temperature gradient and the energy flux resulted by concentration differences is known as thermal-diffusion (Soret) effect and diffusion-thermo (Dufour) effect, respectively. The importance of the S & D effects is visible in many practical applications preferably in areas such as geosciences chemical engineering etc. The S & D effects past a vertical plate embedded in a porous medium in a MHD mixed convection was studied by Makinde[31]. The study of S & D effects over a vertical plate in a mixed convection was conducted by Alam and Rahman[32]. Over a vertical isothermal flat plate Afify[33] studied the effects of a viscosity/temperature parameter, S & D on free convective heat and mass transfer of a viscous fluid. Investigations were carried out by Makinde and Olanrewaju[34] on the unsteady mixed convection with S & D effects past a porous plate moving through a binary mixture of chemically reacting fluid. Further studies were conducted by Beg *et al.*[35] over chemically reacting mixed convective heat and mass transfer along inclined and vertical plates with S & D effects. Combined influence of chemical reaction, heat source, radiation, stretching surface and variable viscosity coupled with

the S & D effects was studied by Tsai and Huang[36] in a porous medium for the Hiemenz flow. El-Arabawy[37] studied the heat and mass transfer by natural convection from vertical surface embedded in a fluid-saturated porous media with S & D effects under variable surface temperature and constant concentration. S & D effects in a MHD free convection boundary layer flow past a semi-infinite moving vertical plate, with suction/injection was investigated by Olanrewaju and Makinde[38] and focusing on viscous dissipation was investigated by Reddy and Reddy[39]. Makinde *et al.*[40] investigated the S & D effects on MHD boundary layer flow over a convectively heated surface. The study of radiation, heat absorption/ generation, heat and mass transfer effects of the unsteady electrically conducting fluid flow past a vertical infinite flat plate with two different types of the thermal boundary conditions was done by Tukyilmazoglu and Pop[41]. Pal and Mondal[42] investigated the influence of thermophoresis and S & D effects on MHD heat and mass transfer over a non-isothermal wedge with thermal radiation and ohmic dissipation. The combined effect of thermophoresis, viscous dissipation and Joule heating on steady MHD flow over an inclined radiative isothermal permeable surface with variable thermal conductivity was investigated by Reddy[43]. The study on unsteady MHD mixed convective flow past an infinite vertical plate with ohmic dissipation and heat source with S & D effects was conducted by Sharma *et al.*[44]. Pal and Mondal[45] focused on S & D effects on MHD non-Darcy convective and radiative heat and mass transfer over a stretching sheet in porous medium with viscous dissipation and ohmic heating. Reddy and Chamkha[46] studied Soret and Dufour effects on unsteady MHD heat and mass transfer from a permeable stretching sheet with thermophoresis and non-uniform heat generation/absorption.

Influenced by the above studies, we set the objective of this paper to study the effect of Joule heating, thermal radiation, radiation absorption, Soret and Dufour parameters and dissipation on the convective heat and mass transfer flow of a conducting viscous fluid past a stretching sheet in the presence of a magnetic field. We investigated the coefficient of heat flux, mass flux and shearing stress at the plate and are analyzed with the specific values of Prandtl number (Pr=0.72). The governing equations, which describe the problem, were transformed and solved numerically using the fourth order Runge–Kutta integration scheme featuring a shooting technique.

2 Problem Formulation

A steady incompressible two-dimensional boundary layer of an electrically conducting fluid spreading over a permeable plane surface has been considered in this paper. An applied magnetic field of strength $B(x)$ is applied transverse to the plate in the y-direction and varies in strength as a function of x. We further consider a Cartesian rectangular co-ordinate system O(x, y) with the plate in the y-direction and x-axis normal to the boundary. The sheet is located at y=0 and its leading edge is the origin of the Cartesian coordinate system. The external electric field assumed to be zero and the magnetic Reynolds number is assumed to be small. Hence the induced magnetic field is small compared with the external magnetic field. Figure 1 shows the sketch of the physical model.

The fluid of density (ρ) is at rest and the motion is created by stretching the sheet with a speed proportional to the distance from the fixed origin (x=0). The dynamic viscosity coefficient (μ) is constant, the pressure gradient and the body forces are negligible in the presence of viscous dissipation and internal heat generation. The effects of uniform mass and heat transfer characteristics in stationary surroundings are investigated. Under these assumptions, the governing equations within the boundary layer are given by:

Continuity equation:

$$\frac{\partial u}{\partial x} + \frac{\partial v}{\partial y} = 0 \qquad \ldots (1)$$

Momentum equation:

$$u\frac{\partial u}{\partial x} + v\frac{\partial u}{\partial y} = \upsilon\frac{\partial^2 u}{\partial y^2} - \frac{\sigma(B(x))^2}{\rho}u + g\beta(T - T_\infty) + g\beta^{\bullet}(C - C_\infty) \qquad \ldots (2)$$

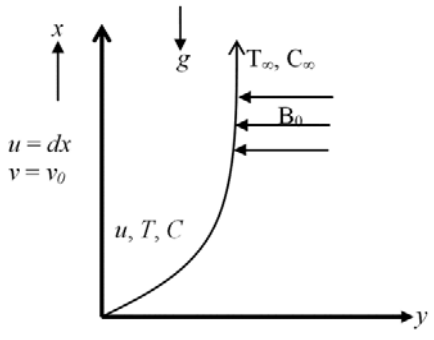

Fig. 1 — Sketch of the physical model.

Energy equation:

$$u\frac{\partial T}{\partial x}+v\frac{\partial T}{\partial y}=\frac{k_f}{\rho C_p}\frac{\partial^2 T}{\partial y^2}+\frac{\mu}{\rho C_p}\left(\frac{\partial u}{\partial y}\right)^2+\frac{\sigma(B(x))^2}{\rho C_p}u^2-\frac{1}{\rho C_p}\frac{\partial q_R}{\partial y}+$$

$$\frac{D_m K_T}{C_s C_p}\frac{\partial^2 C}{\partial y^2}+Q_1^1(C-C_\infty) \quad \ldots (3)$$

Concentration equation:

$$u\frac{\partial C}{\partial x}+v\frac{\partial C}{\partial y}=D_1\frac{\partial^2 C}{\partial y^2}-k_r^{'}(C-C_\infty)+\frac{D_m K_T}{T_m}\frac{\partial^2 T}{\partial y^2} \quad \ldots (4)$$

where u and v are the velocity components along the x and y axes, respectively, υ is kinematic viscosity, T and C are the temperature, concentration in the fluid, T_∞ and C_∞ are ambient temperature, concentration, respectively, k_f is the thermal conductivity, C_p is the specific heat at constant pressure, $k_r^{'}$ is the coefficient of chemical reaction, D_1 is the molecular diffusivity and q_R is the radiative heat flux. The boundary conditions are:

$$u=dx, v=vo, \quad -k_f\frac{\partial T}{\partial y}=q_W(x)=bx^m,$$

$$-D_1\frac{\partial C}{\partial y}=m_W(x)=ax^n, \quad on \quad y=0, \quad \ldots (5)$$

$$u=0\ , \quad T=T_\infty \quad , \quad C=C_\infty \qquad as \qquad y\to\infty$$

Following Rosseland approximation (Raptis[47]) we introduce:

$$q_R=-\frac{4\sigma^\bullet}{3\beta_R}\frac{\partial T^4}{\partial y} \text{ and } T^4\cong 4T_\infty^3 T-3T_\infty^4 \quad \ldots (6)$$

Using Eq. (6), the Eq.(3) reduces to:

$$u\frac{\partial T}{\partial x}+v\frac{\partial T}{\partial y}=\left(\frac{k_f}{\rho C_p}+\frac{16\sigma^\bullet T_\infty^3}{3\beta_R}\right)\frac{\partial^2 T}{\partial y^2}+\frac{\mu}{\rho C_s}\left(\frac{\partial u}{\partial y}\right)^2+\frac{\sigma(B(x))^2}{\rho C_p}u^2+$$

$$\frac{D_m K_T}{C_s C_p}\frac{\partial^2 C}{\partial y^2}+Q_1^1(C-C_\infty) \quad \ldots (7)$$

The above governing non-linear Eqs. (1-7) represent the flow of heat and mass transfer (Tukyilmazoglu and Pop[41]). For the flow under study, it is relevant to assume that the applied magnetic field strength $B(x)$ has the form:

$$B(x)=\frac{B_0}{\sqrt{x}}. \quad \ldots (8)$$

Using Eq. (8), equation of momentum (Eq. (2)) and equation of energy (Eq. (7)) reduces to:

$$u\frac{\partial T}{\partial x}+v\frac{\partial T}{\partial y}=\left(\frac{k_f}{\rho C_p}+\frac{16\sigma^\bullet T_\infty^3}{3\beta_R}\right)\frac{\partial^2 T}{\partial y^2}+\frac{\mu}{\rho C_s}\left(\frac{\partial u}{\partial y}\right)^2+\frac{\sigma(B_0(x))^2}{\rho C_p}u^2+$$

$$\frac{D_m K_T}{C_s C_p}\frac{\partial^2 C}{\partial y^2}+Q_1^1(C-C_\infty) \quad \ldots (9)$$

From Eq. (8) and Eq. (2) the momentum equation can be rewritten as:

$$u\frac{\partial u}{\partial x}+v\frac{\partial u}{\partial y}=\upsilon\frac{\partial^2 u}{\partial y^2}-\frac{\sigma_0 B_o^2}{\rho x}u+g\beta(T-T_\infty)+g\beta^\bullet(C-C_\infty) \quad \ldots (10)$$

In view of the continuity Eq. (1) we define a stream function $\psi(x,y)$ as:

$$u=\frac{\partial\psi}{\partial y}\ , \quad v=-\frac{\partial\psi}{\partial x} \quad \ldots (11)$$

Using Eq. (11) we find that:

$$u=dxf'(\eta), \quad v=-\sqrt{d\upsilon}f(\eta) \quad \ldots (12)$$

where prime denote differentiation with respect to η. The following transformations are introduced:

$$\eta=\sqrt{\frac{d}{\upsilon}}y\ , \quad \psi=\sqrt{d\upsilon}xf(\eta), \quad T-T_\infty=\frac{D}{k_f}\sqrt{\frac{\upsilon}{d}}\left(\frac{x}{L}\right)^2\theta(\eta),$$

$$C-C_\infty=\frac{D_2}{D_1}\sqrt{\frac{\upsilon}{d}}\left(\frac{x}{L}\right)^2\phi(\eta) \quad \ldots (13)$$

The momentum, energy and concentration equations can be written in similarity variables as:

$$f'''-(f')^2+ff''-M^2f'+\frac{G}{R_{ex}^2}(\theta+N\phi)=0 \quad \ldots (14)$$

$$\frac{1}{\Pr}\left(1+\frac{4Nr}{3}\right)\theta''+Ec(f'')^2-2\theta f'+f\theta'+EcM^2(f')^2+Q_1\phi+Du\phi''=0 \quad \ldots (15)$$

$$\phi''+(f\phi'-2f'\phi)-(k_r)\phi+Sr\theta''=0\ . \quad \ldots (16)$$

Following Nachtsheim and Swigert[48], transformed boundary conditions may be written as:

$$f(0)=f_W, f'(0)=1, \theta'(0)=-(b/a)L^2x^{m-2}=-1, \phi'(0)=-(aL^2/D_2)x^{n-2}=-1,$$

$$f'(\infty)=0, \theta(\infty)=0, \ \phi(\infty)=0, \quad \ldots (17)$$

But as $\theta'(0)$, $\phi'(0)$ must be equal to -1, this implies (as could be concluded from Eq. (17)) that m=2, n=2, a and b must satisfy the following relations:

$$b=\frac{D_2}{L^4}\ , \quad a=\frac{D_2}{L^2} \quad \ldots (18)$$

where $f_w = -v_0/(d\upsilon)^{1/2}$ is the dimensionless wall mass transfer coefficient such that $f_w>0$ indicates wall suction and $f_w< 0$ indicates wall injection. The following parameters are used in the Eqs (14)-(16):

$R_{ex} = \frac{dx^2}{\nu}$ (Local Reynolds number)

$S_r = \frac{D_m D_1 DK_T}{D_2 T_m}$ (Soret parameter)

$G = \frac{\beta g \Delta T x^3}{\nu^2}$ (Grashof number)

$Du = \frac{DmD_2 K_T K_f}{D_1 DC_s C_p}$ (Dufour parameter)

$N = \frac{\beta^{\bullet} D_2 k_f}{\beta DD_1}$ (Buoyancy number)

$Nr = \frac{4\sigma^{\bullet} T_\infty^3}{\beta_R K_f}$ (Thermal radiation parameter)

$M^2 = \frac{\sigma_0 B_0^2}{\rho}$ (Magnetic parameter)

$k_r = \frac{k_r' \upsilon}{d}$ (Chemical reaction parameter)

$Ec = \frac{k_f}{D}\frac{L^2}{\sqrt{d\upsilon}}\frac{d^3}{C_p}$ (Eckert number)

$\Pr = \frac{\mu C_p}{k_f}$ (Prandtl number)

Using Ahammad and Mollah[49] the other physical quantity of interest is the local skin friction (C_f), local Nusselt number (Nu) and the local Sherwood number (Sh) may be written as:

Local skin friction:

$$\tau_w = \{(\mu)\frac{\partial u}{\partial y}\}_{y=0} = \mu d\sqrt{\frac{d}{\nu}} xf''(0)$$

It is clear that the wall shear stress will increase with increasing x. The skin friction coefficient C_f takes the form:

$$C_f = \frac{\tau_w}{0.5\rho(dx)^2} = \frac{2}{(R_{ex})^{1/2}}[f''(0)]$$

$$\frac{1}{2} Cf_x (R_{ex})^{1/2} = f''(0) \quad \ldots (19)$$

Local Nusselt number:

$$Nu_x (R_{ex})^{-1/2} = \frac{1}{\theta(0)} \quad \ldots (20)$$

Local Sherwood number:

$$Sh_x (R_{ex})^{-1/2} = \frac{1}{\phi(0)} \quad \ldots (21)$$

3 Numerical Procedures

The system of non-linear ordinary differential Eqs. (14-16) together with the boundary conditions (Eq. 17) has been numerically solved by using Nachtsheim-Swigert shooting iteration technique (guessing the missing value) along with sixth order Runge-Kutta initial value solver (Alam and Ahammad[50]). In a shooting method, the missing (viz., unspecified) initial condition at the initial point of the interval is assumed, and the differential equation is then integrated numerically as an initial problem to the terminal point. The accuracy of the assumed missing initial condition is then checked by comparing the calculated value of the dependent variable at the terminal point with its given value there. If a difference exists, another value of the missing initial condition must be assumed and the process is repeated. This process is continued until the agreement between the calculated and the given condition at the terminal point is within the specified degree of accuracy. In this type of iterative approach, it is pertinent to know whether there is a symmetric way of finding each succeeding value (assumed value) of the initial condition.

The method of numerically integrating a two-point asymptotic boundary value problem of the boundary-layer type, the initial value method is similar to an initial value problem. Thus it is necessary to estimate as many boundary conditions at the surface as were given at infinity. The governing differential equations are then integrated with these assumed surface boundary conditions. If the required outer boundary condition is satisfied, a solution has been achieved. However, this is not generally the case. Hence, a method must be devised to estimate logically the new surface boundary conditions for the next trial integration. Asymptotic boundary value problems such as those governing the boundary-layer equations are further complicated by the fact that the outer boundary condition is specified at infinity. In the trial integration, infinity is numerically approximated by

Table 1 — Comparison of skin friction (C_f), heat flux (Nu) and mass flux (Sh) for our α= 90, f_w=0.2, Sc=1.3, Nr=0, Ec=0 case with different Sr and Du with Alam *et al.*[50]

Sr	Du	Literature[50]			Present results (numerical values)		
		C_f	Nu	Sh	C_f	Nu	Sh
2	0.03	3.3565689	1.4361584	0.6767115	3.356569	1.436158	0.676712
1	0.06	3.1145821	1.4024461	0.7542388	3.114582	1.402446	0.754239
0.5	0.12	3.0271220	1.3662225	0.8023145	3.027122	1.366222	0.802314

Table 2 — Comparison of heat transfer (1/θ(0)) with Elbashbeshy[51] and Chen[52] of their Newtonian fluid case for f_w=0.6, Sc=0.22 and M=Q_1=Ec=Nr=Sr=Du=0 for our different values of Pr

Pr	Literature[51]	Literature[52]	Present values
0.72	0.7711	0.76217	0.7622077
1.00	1.00060	1.00616	1.0062479
10.00	7.0921	7.09295	7.092874

some large value of the independent variable. There is no a prior genera method of estimating these values. Selecting too small maximum value for the independent variable may not allow the solution to asymptotically converge to the required accuracy. In Eq. (17) there are three asymptotic boundary conditions and hence three unknown surface conditions $f''(0)$, $\theta'(0)$ and $\phi'(0)$.$\Delta\eta$ = 0.01 were selected as the step size that satisfied a convergence criterion of 10^{-6} for the calculations of parameters in different phases.

4 Comparison

In the absence of viscous dissipation Ec=0 and thermal radiation Nr=0, the results obtained herein are compared with Alam and Ahammad[50]. To assess the accuracy of the present numerical method, we have compared the results of our rate of heat transfer (1/θ(0)) with those of Elbashbeshy[51] and Chen[52] for their Newtonian fluid case, in the absence of M, Q_1, Ec, Nr, Sr, Du for different values of Pr in Table 1 and Table 2 and the results are found to be in excellent agreement.

5 Results and Discussion

In order to get a clear insight of the physical problem, numerical results are displayed with the help of graphical illustrations. The results are given through a parametric study showing the influence of several non-dimensional parameters, Hartmann number M, Eckert number Ec, radiation absorption parameter Q_1, thermal radiation parameter Nr, Soretparameter Sr, Dufour parameter Du, Prandtl number Pr, suction parameter fw, buoyancy ratio N, chemical reaction parameter γ and heat source parameter Q. The non-linear equations governing the flow, heat and mass transfer have been solved numerically by employing sixth order Runge–Kutta shooting method. The sheet is assumed to be non-isothermal with prescribed heat flux varying with length.

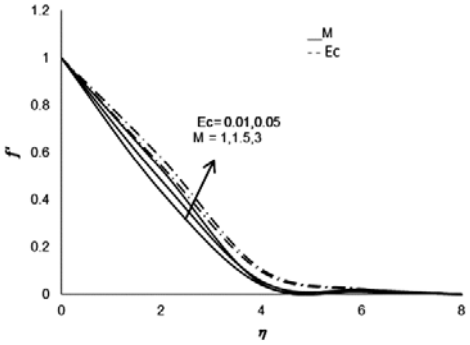

Fig. 2 — Effect of Hartmann number (M) and Eckert number (Ec) on velocity profiles.

The velocity (f'), temperature (θ) and concentration (ϕ) are plotted versus η for the values M=1, Ec=0.01, Q_1=0.5, Nr=1, Sr=2, Du=0.01, Pr=0.71, f_w=2, N=0.5, γ=0.5, Q=0.5 and specific variations of physical parametric values are varies unless remain same. We follow the convention that the non-dimensional temperature or concentration is positive or negative according to the actual temperature or concentration that is greater or lesser than T_∞/C_∞.

5.1 Velocity profiles

Figure 2 represents the axial velocity (f') with Hartmann number M. It can be seen from the profiles that the axial velocity reduces with increase in M≤1.5 and enhances with higher M≥3. This is due to the fact that the magnetic field provides a resisting type of force known as the Lorentz force. This force tends to lesser the motion of the fluid and as a consequence the velocity reduces. The variation of f' with Ec shows that the axial velocity enhances with increasing values of Ec owing to the energy release which increases the

momentum. Figure 3 represents (f') with radiation absorption parameter, Q_1 and thermal radiation parameter, Nr. It is found that there is a significant depreciation in f', in the presence of the thermal radiation throughout the boundary layer. The radiation parameter is found to reduce the hydrodynamic boundary layer along the x-direction. An increase in Q_1 reduces the velocity f'. This is due to the fact that the thickness of the momentum boundary layer reduces with increasing Q_1. Figure 4 shows the variation of f'' with Soret parameter (Sr) or Dufour parameter (Du). It can be seen from the profiles that the increasing the Soret parameter (Sr) (or decreasing Dufour parameter (Du)) reduces the velocity f'' with reference to Prandtl number (Pr). We find that the velocity f'' shows a reduction for increasing values of Prandtl number and hence the thickness of the boundary layer also reduces. Figure 5 represents f'' with suction parameter f_w and buoyancy ratio (N). It is found that when the molecular buoyancy force dominates over the thermal buoyancy force, the velocity f'' enhances when the buoyancy forces are in the same direction and for the forces acting in opposite direction f'' reduces in the boundary layer. An increase in the suction/injection parameter f_w enhances the velocity f'. This is due to the fact the thickness of the momentum boundary layer increases with increasing f_w. Figure 6 represents f'' with chemical reaction parameter γ. It can be seen from the profiles that f'' enhances in both degenerating/generating chemical reaction cases. Figure 7 shows f'' with heat source parameter Q. The velocity f'' enhances with increasing values of heat generation/absorption. This is due to the fact that the presence of the heat source/sink generates

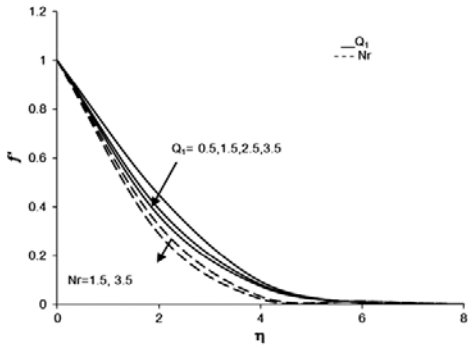

Fig. 3 — Effect of aadiation absorption parameter (Q_1) and thermal radiation parameter (Nr) on velocity profiles.

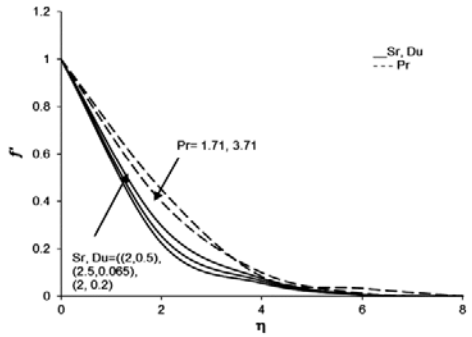

Fig. 4 — Effect of Soret (Sr), Dufour parameter (Du) and Prandtl number (Pr) on velocity profiles.

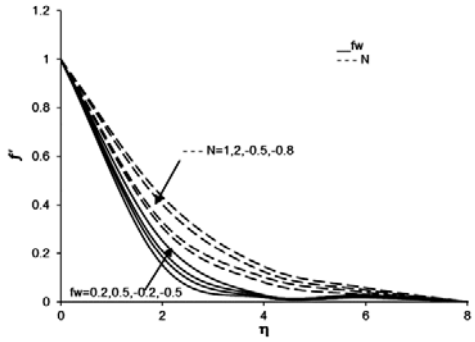

Fig. 5 — Effect of suction parameter (f_w) and Buoyancy ratio (N) on velocity profiles.

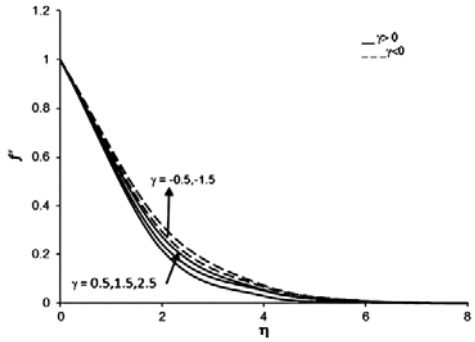

Fig. 6 — Effect of chemical reaction parameter (γ) on velocity profiles.

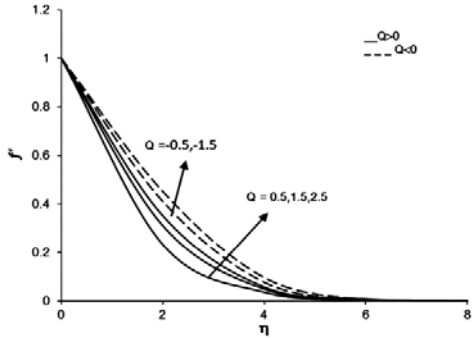

Fig. 7 — Effect of heat source parameter (Q) on velocity profiles.

energy in the thermal boundary layer and as a consequence the temperature rises.

5.2 Temperature profiles

Figure 8 illustrates the temperature (θ) with Hartmann number, *M*. The temperature enhances with *M*. This is due to the fact an increase in *M* results in the reduction of velocity and thereby enhances the temperature in the thermal boundary layer. From Fig. 8 we find that an increase in Eckert number, *Ec*. Figure 9 illustrates temperature (θ) Q_1 and *Nr*. The presence of thermal radiation is very significant on the variation of temperature. It is seen that the temperature enhances gradually in the presence of thermal radiation parameter *Nr* throughout the boundary layer. This may be attribute the fact that as the Rosseland radiative absorption parameter diminishes the corresponding heat flux diverse and thus reduces the rate of radiative heat transfer to the fluid causing a rise in the temperature of the fluid. The thickness of the boundary layer also reduces in the presence of Nr. An increase in Q_1 leads to a rise in the temperature in the fluid.

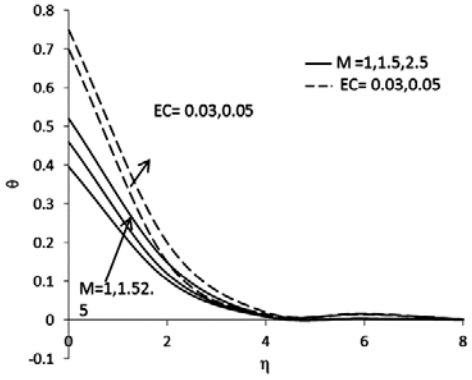

Fig. 8 — Effect of Hartmann number (*M*) and Eckert number (*Ec*) on temperature profiles.

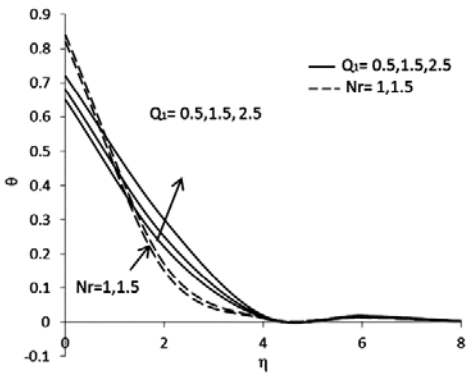

Fig. 9 — Effect of radiation absorption parameter (*Q*1) and thermal radiation parameter (*Nr*) on temperature profiles.

Figure 10 shows the variation of temperature (θ) with *Sr*, *Du* and *Pr*. It can be seen from the profiles that the temperature reduces with increasing Soret parameter *Sr* (or decreasing Dufour parameter *Du*). As Prandtl number increases there is a significant increase in the thermal boundary layer with a rise in the temperature throughout the boundary layer, since enhancement of Prandtl number amounts to enhancement of thermal-diffusion. Figure 11 represents temperature (θ) with suction parameter f_w. An increase in suction/injection parameter f_w reduces the temperature. Figure 12 illustrate temperature (θ) with chemical reaction parameter γ. It can be observed from the profiles that the temperature enhances with increase in generating chemical reaction case whereas temperature reduces in the degenerating chemical reaction case. Figure 13 represents temperature (θ) with heat source parameter *Q*. The presence of heat source generates, absorbs in the thermal boundary layer and as a consequence the temperature rises while it reduces with increase in the heat sink. This is due to the fact that the

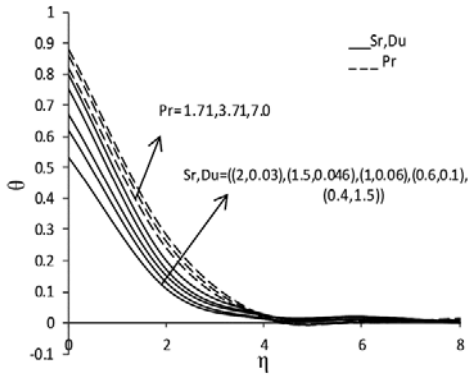

Fig. 10 — Effect of Soret (*Sr*), Dufour parameter (*Du*) and Prandtl number (*Pr*) on temperature profiles.

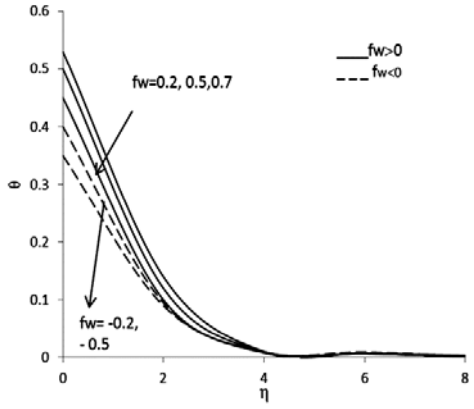

Fig. 11 — Effect of Suction parameter (*f*w) on temperature profiles.

energy is absorbed in the boundary layer. Figure 14 represents the temperature (θ) with buoyancy ratio (*N*). It is found that when the molecular buoyancy force dominates over the thermal buoyancy force the temperature enhances in the boundary layer irrespective of the directions of the buoyancy forces.

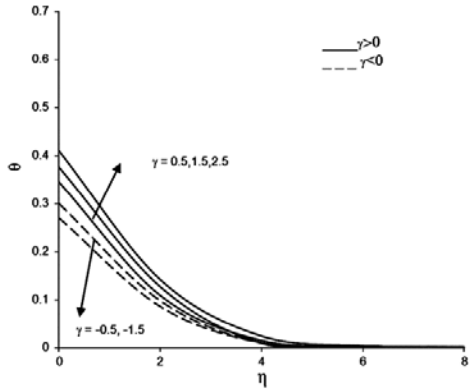

Fig. 12 — Effect of chemical reaction parameter (γ) on temperature profiles.

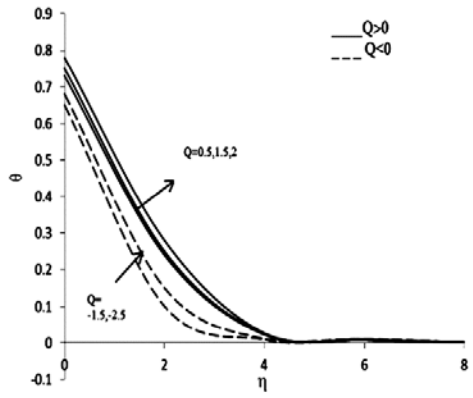

Fig. 13 — Effect of heat source parameter (*Q*) on temperature profiles.

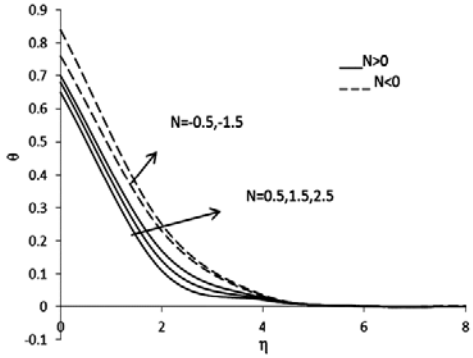

Fig. 14 — Effect of Buoyancy ratio (*N*) on temperature profiles.

5.3 Concentration profiles

Figure 15 illustrates the concentration distribution, ϕ with Hartmann number, *M*. It can be same seen from the profiles that the concentration that enhances with increase in *M*. The variation of concentration ϕ with Eckert number *Ec* shows that the concentration increases with increase in *Ec*. It is due to the fact that the thermal energy is reserved in fluid on account of friction heating. Hence the concentration distribution rises in the entire solute boundary layer. Figure 16 shows the variation of concentration distribution ϕ with Q_1 and *Nr*. We find that higher the radiative heat flux larger the concentration. An increase in Q_1 results depreciation in the concentration. It is due to the fact that the thickness of the solutal boundary layer increases with Q_1. Figure 17 illustrates the concentration distribution ϕ with *Sr* (decrease in Dufour parameter *Du*) and *Pr*. Increasing the Soret parameter *Sr* (or decreasing Dufour parameter *Du*) leads to depreciation in the concentration. It is due to the fact that the thickness of the boundary layer reduces with increase in the *Sr*. The mass concentration increases with *Pr*. As a Prandtl

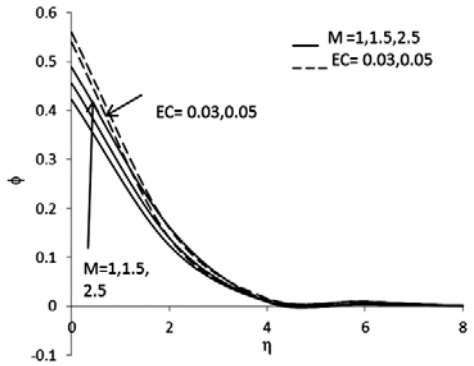

Fig.15 — Effect of Hartmann number (*M*) and Eckert number (*Ec*) on concentration profiles.

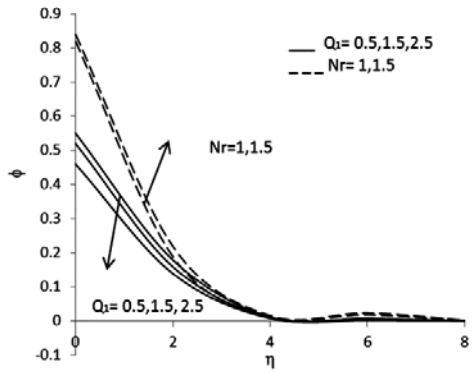

Fig.16 — Effect of radiation absorption parameter (Q_1) and thermal radiation parameter (*Nr*) on concentration profiles.

number increases there is a significance increase in the solutal boundary layer thickness with a rise in the concentration throughout the boundary layer, since enhancement of Prandtl number enhances of concentration diffusion. Figure 18 represent concentration distribution ϕ with suction parameter f_w. Increase in suction parameter $f_w>0$ enhances the concentration and reduces with injection parameter $f_w<0$. With respect to chemical reaction parameter γ, we notice an enhancement in concentration in both degenerating and generating chemical reaction cases throughout the boundary layer is illustrated in Fig. 19.

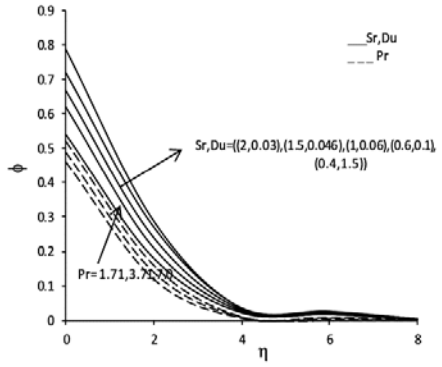

Fig. 17 — Effect of Soret (*Sr*), Dufour parameter (*Du*) and Prandtl number (*Pr*) on concentration profiles.

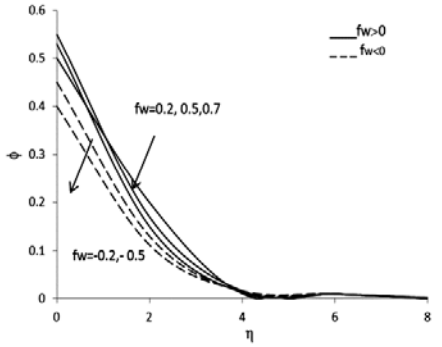

Fig. 18 — Effect of suction parameter (f_w) on concentration profiles.

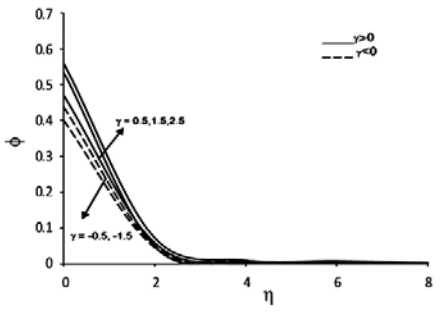

Fig. 19 — Effect of chemical reaction parameter (γ) on concentration profiles.

Figure 20 illustrates concentration distribution ϕ with heat source parameter *Q*. In the presence of heat source energy is generated in the boundary layer which leads to a rise in the concentration whole the concentration reduces with decrease in the heat sink parameter $Q<0$. This is due to the fact that heat is absorbed in the boundary layer. Figure 21 illustrates concentration distribution (ϕ) with buoyancy ration (*N*). When the molecular buoyancy force dominates the thermal buoyancy force the concentration reduces in boundary layer, when the buoyancy forces are in the same direction and for the forces acting in opposite directions, it enhances in the boundary layer.

5.4 Skin friction, Nusselt number and Sherwood number

The dimensionless wall values of velocity, temperature and concentrations are graphically represented for various parameters *Nr*, *Ec*, f_w, Q_1, *Sr* and *Du* are illustrated through the graphical notation. The skin friction components C_f, Nusselt number *Nu* and Sherwood number *Sh* have been plotted in Figs 22-30.

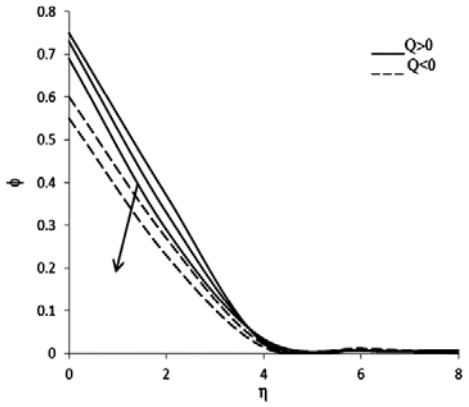

Fig. 20 — Effect of heat source parameter (*Q*) on concentration profiles.

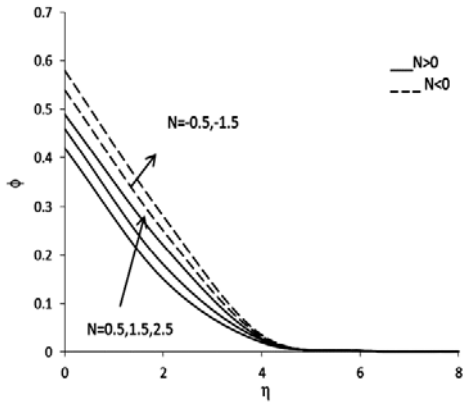

Fig. 21 — Effect of Buoyancy ratio (*N*) on concentration profiles.

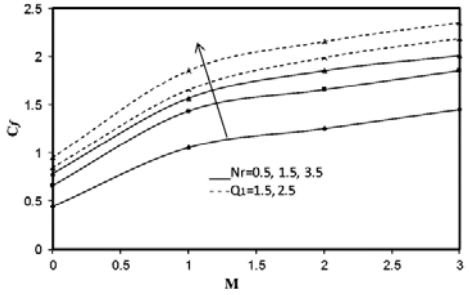

Fig. 22 — Effects of thermal radiation parameter (Nr) and radiation and absorption parameter (Q_1) on skin friction coefficient (C_f) for Ec=0.01, Sr=2, Du=0.01, Pr=0.71, f_w=2, N=0.5, γ=0.5, Q=0.5.

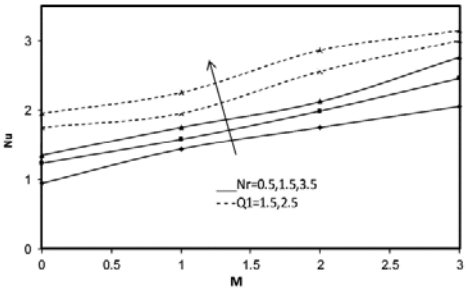

Fig. 23 — Effects of thermal radiation parameter (Nr) and radiation and absorption parameter (Q_1) on Nusselt number (Nu), for Ec=0.01, Sr=2, Du=0.01, Pr=0.71, f_w=2, N=0.5, γ=0.5, Q=0.5.

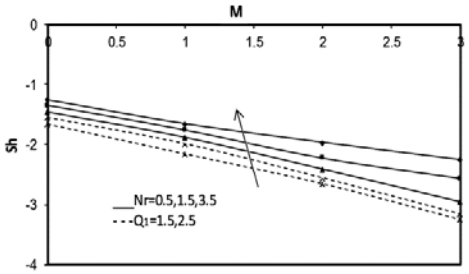

Fig. 24 — Effects of thermal radiation parameter (Nr) and radiation and absorption parameter (Q_1) on Sherwood number for Ec=0.01, Sr=2, Du=0.01, Pr=0.71, f_w=2, N=0.5, γ=0.5, Q=0.5.

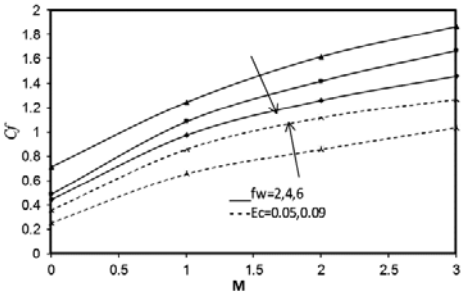

Fig. 25 — Effects of suction parameter (f_w) and Eckert number (Ec) on skin friction coefficient (C_f) for Nr=0.5, Q_1=0.5 Sr=2, Du=0.01, Pr=0.71, N=0.5, γ=0.5, Q=0.5.

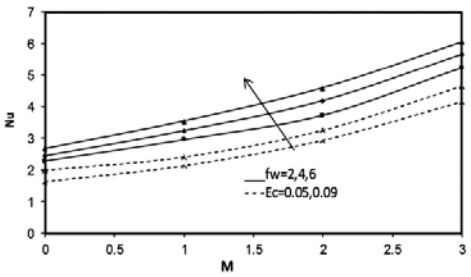

Fig. 26 — Effects of suction parameter (f_w) and Eckert number (Ec) on Nusselt number for Nr=0.5, Q_1=0.5, Sr=2, Du=0.01, Pr=0.71, N=0.5, γ=0.5, Q=0.5.

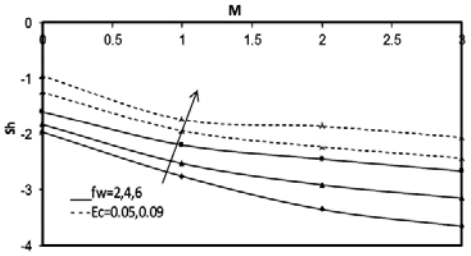

Fig. 27 — Effects of suction parameter (f_w) and Eckert number (Ec) on Sherwood number for Nr=0.5, Q_1=0.5, Sr=2, Du=0.01, Pr=0.71, N=0.5, γ=0.5, Q=0.5.

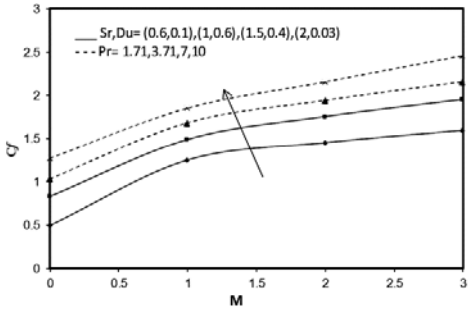

Fig. 28 — Effects of Soret (Sr) and Dufour (Du) parameter and Prandtl number (Pr) on skin friction coefficient (C_f) or Nr=0.5, Q_1=0.5, f_w=2, Ec=0.01, N=0.5, γ=0.5, Q=0.5.

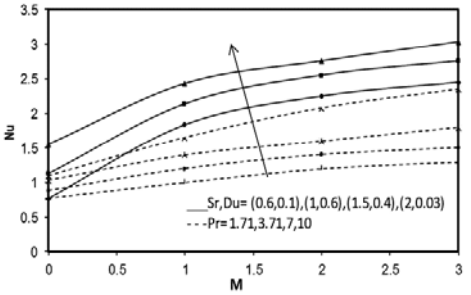

Fig. 29 — Effects of Soret (Sr) and Dufour (Du) parameter and Prandtl number (Pr) on Nusselt number (Nu) for Nr=0.5, Q_1=0.5, f_w=2, Ec=0.01, N=0.5, γ=0.5, Q=0.5.

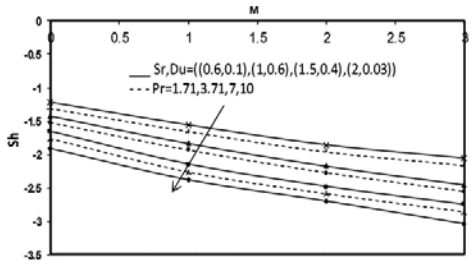

Fig. 30 — Effects of Soret (*Sr*) and Dufour (*Du*) parameter and Prandtl number (*Pr*) on Sherwood number (*Nu*) for *Nr*=0.5, *Q*1=0.5, f_w=2, *Ec*=0.01, *N*=0.5, γ=0.5, *Q*=0.5.

Skin friction parameter C_f, enhances with increase in *Nr*, *Ec* and Q_1 and reduces with f_w. An increase in Prandtl number *Pr*, Soret parameter *Sr* (or decrease in Dufour parameter *Du*) results depreciation in $C_f$at the wall.

The rate of heat transfer (local Nusselt number *Nu*) enhances with increase in f_w. Higher the radiative heat flux or radiation absorption or heat dissipation larger |*Nu*| at the wall. The variation of *Nu* with *Pr*, *Sr* and *Du* shows that the rate of heat transfer reduces with increase in *Sr* (or decrease in Dufour parameter *Du*). The rate of mass transfer (local Sherwood Number *Sh*) shows that the rate of mass transfer enhances with f_w. Also higher the radiative heat flux or radiative absorption or heat dissipation larger the rate of mass transfer at the wall. Increase in the, Prandtl number *Pr*, Soret parameter *Sr* (or decrease in the Dufour parameter, *Du*) results in decrease in the rate of mass transfer at the wall.

6 Conclusions

We investigated the coefficient of heat flux, mass flux and shearing stress at the plate and are analyzed with the specific values of Prandtl number (*Pr*=0.71, 1.71, 3.71, 5). Graphical results for various parametric conditions were presented and discussed for different values. The main findings are summarized as follows:

The velocity f' increases with the increase in thermal radiation *Nr*, Eckert number *Ec*, suction parameter f_w in the entire flow region, while the radiation absorption parameter Q_1 and Soret *Sr* (decreasing in Dufour *Du*) parameters reduces the thermal boundary layer in the entire flow region.

The temperature θ falls with rise in Soret/Dufour parameter, Eckert number *Ec*. Whereas temperature increases with rise in radiation absorption parameter Q_1, Prandtl number *Pr* and thermal radiation *Nr* in the flow region. The temperature θ increases in both suction (f_w>0) and injuction parameter (f_w<0) in the entire flow field.

The generating chemical reaction parameter and degenerating chemical reaction parameter increases with increase in the temperature. The molecular buoyancy forces dominates the thermal buoyancy force, the temperature enhances in the entire boundary layer.

The influence in radiation absorption parameter Q_1, suction parameter f_w and Soret or Dufour parameters causes depreciation in the concentration in the entire flow field. Whereas, the effect of concentration experiences an enhancement with increasing f_w>0 and depreciation with f_w<0. With increase inEckert number *Ec*,thermal radiation parameter *Nr*, Soret parameter *Sr* (or decrease in Dufour parameter) the concentration ϕ experiences an enhancement in the entire flow region.

Skin friction C_f enhances with increase in thermal radiation parameter *Nr*, Eckert number *Ec*, radiation absorption parameter Q_1, Prandtl number Prand C_f reduces with increase in suction parameter f_w, Soret parameter *Sr* (or decrease in Dufour parameter *Du*) at the wall.

The rate of heat transfer enhances with increase in suction parameter f_w. With increase in radiative heat flux or radiation absorption or heat dissipation |Nu| increases at the wall. The rate of heat transfer reduces with increase in Soret parameter *Sr* (or decrease in Dufour parameter *Du*).

The rate of mass transfer enhances with increase in suction parameter f_w, radiative heat flux, radiative absorption, heat dissipation and Prandtl number at the wall. An increase in Soret parameter *Sr* (or decrease in Dufour parameter *Du*) results a depreciation in the rate of mass transfer at the wall.

References

1 Hossain M A, *Int J Heat Mass Trans*, 35 (1992) 3485.
2 Mamun A A, Chowdhury Z R, Azim M A & Molla M M, *Int Commun Heat Mass Trans*, 35 (2008) 1275.
3 Palani G & Kwang Y K, *J Eng Thermophys*, 20 (2011) 501.
4 Makinde O D & Chinyoka T, *Commun Nonlinear Sci Numer Simul*, 15 (2010) 3919.
5 Das S, Jana R N & Makinde O D, *Alexandria Eng J*, 54 (2015) 251.
6 Makinde O D, Khan W A & Culham J R, *Int J Heat Mass Trans*, 93 (2016) 595.
7 Makinde O D, *Can J Chem Eng*, 88 (2010) 983.
8 Hossain M A & Alim M A, *J Heat Mass Trans*, 32 (1997) 515.
9 Hossain M A & Takhar H S, *J Heat Mass Trans*, 35 (1999) 321.
10 Anjali Devi S P & Thiyagarajan E M, *J Heat Mass Trans*, 42 (2006) 671.
11 Mukhopadhyay S & Andersson H I, *J Heat Mass Trans*, 45 (2009) 1447.

12 Makinde O D, *Z Naturforsch*, 67a (2012) 239.
13 Cortell R, *Meccanica*, 47 (2012) 769.
14 Makinde O D, Mabood F, Khan W A & Tshehla M S, *J Mol Liq*, 219 (2016) 624.
15 Khan W A & Makinde O D, Khan Z H, *Int J Heat Mass Trans*, 96 (2016) 525.
16 Pal D, *Int J Comput Meth Eng Sci Mech*, 16 (2015) 170.
17 Sivaraj R & Kumar R B, *Int J Appl Math Phys*, 4 (2012) 93.
18 Turkyilmazoglu M, *Int J Heat Mass Trans*, 90 (2015) 781.
19 Vajravelu K & Hadjinicolaou A, *Int Commun Heat Mass Trans*, 20 (1993) 417.
20 Chen C H, *Int J Eng Sci*, 42 (2004) 699.
21 Sharma P R & Singh G, *Therm Sci*, 13(1) (2009) 5.
22 Singh A K & Gorla R S R, *Heat Mass Trans*, 45 (2009)1341.
23 Pal D & Talukdar B, *Commun Nonlinear Sci Numer Simul*, 15 (2010) 2878.
24 Babu V S H & Reddy G V R, *Int J Adv Appl Sci Res*, 2 (2011) 138.
25 Babaelahi M, Domairry G & Joneidi A A, *Meccanica*, 45 (2010) 817.
26 Raju K V S, Reddy S T, Raju M C, Satyanarayana P V & Venkataramana S, *Ain Shams Eng J*, 5 (2014) 543.
27 Khader M M & Ahmed M M, *Transport Porous Med*, 105 (2014) 487.
28 Motsumi T G & Makinde O D, *Phys Scripta*, 86 (2012) 045003.
29 Pal D & Mondal G, *Powder Technol*, 279 (2015) 61.
30 Turkyilmazoglu M, *AIP Phys Fluids*, 28 (2016) 043102.
31 Makinde O D, *Lat Am Appl Res*, 41 (2011) 63.
32 Alam M S & Rahman M M, *Nonlinear Anal Model*, 11 (2006) 3.
33 Afify A A, *Transport Porous Med*, 66 (2007) 391.
34 Makinde O D & Olanrewaju P O, *Chem Eng Commun*, 198(7) (2011) 920.
35 Beg O A, Beg T A, Bakier A Y & Prasad V R, *Int J Appl Math Mech*, 5(2) (2009) 39.
36 Tsai R & Huang J S, *Int J Heat Mass Trans*, 52 (2009) 2399.
37 El-Arabawy H A M, *J Math Stat*, 5(3) (2009) 190.
38 Olanrewaju P O & Makinde O D, *Arab J Sci Eng*, 36 (2011) 1607.
39 Reddy G M & Reddy B N, *Int J Appl Math Mech*, 6(1) (2010) 1.
40 Makinde O D, Zimba K & Bég A O, *Int J Therm Environ Eng*, 4(1) (2012) 89.
41 Tukyilmazoglu M & Pop I, *Int J Heat Mass Trans*, 55 (25-26) (2012) 7635.
42 Pal D & Mondal H, *J Magn Magn Mater*, 331 (2013) 250.
43 Reddy M G, *J Appl Fluid Mech*, 7(1) (2014) 51.
44 Sharma B K, Gupta S, Vamsikrishna V & Bhargavi R J, *Afrika Mathematika*, 25 (2014) 799.
45 Pal D & Mondal H, *J Appl Fluid Mech*, 7(3) (2014) 513.
46 Reddy P S & Chamkha A J, *J Appl Fluid Mech*, 9(5) (2016) 2443.
47 Raptis R, *Int Commun Heat Mass Trans*, 25 (1998) 289.
48 Nachtsheim P R & Swigert P, NASA TND-3004 (1965).
49 Ahammad M U & Mollah S H, *Int J Eng Technol*, 11(5) (2011) 4.
50 Alam M S & Ahammad M U, *Nonlinear Anal Model*, 16(1) (2011) 1.
51 Elbashbeshy E M A, *J Phys D: Appl Phys*, 31 (1998) 1951.
52 Chen C H, *Int J Therm Sci*, 47(7) (2008) 954.